Blue emitting C_2-symmetrical dibenzothiazolyl substituted pyrrole, furan and thiophene

Brodie L. Reid,[a] Steven B. Briggs,[a, b] Louise E. Karagiannidis,[a, b] Sara Muzzioli,[c] Paolo Raiteri,[a] Mark E. Light,[b] Stefano Stagni,[c, *] Pierpaolo Brulatti,[d] Philip A. Gale,[b] Mark I. Ogden,[b] Massimiliano Massi[a, *]

The synthesis and photophysical properties of pyrrole, furan and thiophene substituted in their 2 and 5 positions by 2′-benzothiazolyl moieties have been investigated. The three species show deep-blue fluorescence with maxima in the 444-450 nm region, originating from excited states of π-π* character. The photoluminescence quantum yields were found to be higher for the pyrrole and furan compounds, 0.42 and 0.47 respectively, compared to the quantum yield of the thiophene species, 0.21. Light Emitting Devices were fabricated using the pyrrole species as 4% dopant in a 4,4',4"-tri(9-carbazoyl)triphenylamine emissive layer, or the same pyrrole species as a neat film. In low concentration of dopant, the device is characterised by deep-blue emission with CIE coordinates of x=0.182, y=0.185; on the other hand, a neat film of the dopant produces white light emission with CIE x=0.381, y=0.400 but at a cost of quantum efficiency due to self-quenching

Introduction

Benzothiazole and benzothiazolyl-containing species have attracted significant attention due to the optical properties associated with their electronic excited states. These species have been investigated in a variety of fields for many potential applications, including strongly fluorescent molecules with emission in the entire visible spectrum,[1-6] ligands for phosphorescent coordination complexes including transition metals[7-10] and as antennae for lanthanoid elements,[11-13] non-linear optics,[14, 15] photochromic sensors[16] as well as electron-transporting groups and fluorescent dopants in the fabrication of organic light emitting devices (OLEDs).[17-19]

The attachment of benzothiazolyl substituents to five-membered heterocycles including pyrrole, furan and thiophene has been reported in detail by de Melo and Raposo.[3, 5, 14, 15, 20, 21] These studies were mainly focused on the emissive and non-linear optics properties of non-symmetric donor-acceptor molecular species, with the benzothiazole moiety serving as the electron acceptor substituent. In our studies, we have previously reported the synthesis of 2,5-(dibenzothiazol-2-yl) substituted pyrrole **1** (Figure 1) as a ligand for cobalt and copper complexes.[22] These systems are analogous to the previously reported donor-acceptor species, with the difference that in our case the molecular species are symmetrical due to the equivalent substitution of the pyrrole ring in positions 2 and 5 by two identical benzothiazole moieties. In a preliminary investigation, we reported the steady state photophysical properties of this species, which revealed blue fluorescent emission upon excitation at λ_{ex}=385 nm.[22] Prompted by these findings, we have continued this investigation with the synthesis of the 2,5-(dibenzothiazol-2-yl)furan and thiophene analogues **2** and **3** (Figure 1) and we have examined their photophysical properties in detail. Moreover, compound **1** was tested as an emissive dopant for the fabrication of OLEDs.

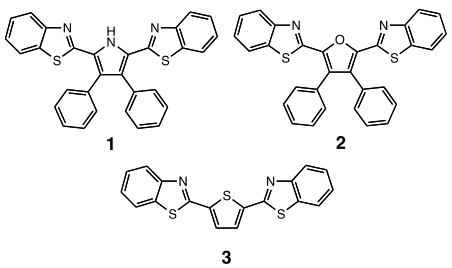

Figure 1. Representation of the 2,5-(dibenzothiazol-2-yl) substituted pyrrole, furan, and thiophene species prepared in this work.

Experimental Section

General details

Solvents and reagents were purchased from Sigma Aldrich and used as received without any further purification. 2,5-bis(*N*-phenyl thioamide)-3,4-diphenylfuran, 2,5-bis(*N*-phenyl thioamide)thiophene, and **1** were prepared according to previously published procedures.[22-24] The purification of compounds **2** and **3** was performed via column chromatography using silica gel as the stationary

phase (Grace, LC60A 40-63 μm). ^{1}H and ^{13}C NMR spectra were measured using a Bruker Avance 400 spectrometer (400.1 MHz for ^{1}H, 100.0 MHz for ^{13}C) at room temperature. Chemical shifts were referenced to residual solvent resonances. IR spectra were obtained from solid-state samples, on an attenuated total reflectance Perkin Elmer Spectrum 100 FT-IR with a diamond stage. Band intensities are reported as strong (s), medium (m), weak (w). Elemental analyses were performed by CMAS (Melbourne, Australia). The values were corrected for the presence of residual solvent (dichloromethane) from the chromatographic purification. Melting points were determined using a BI Barnsted Electrothermal 9100 apparatus. X-ray diffraction data were collected on a Nonius KappaCCD. Following analytical absorption corrections and solution by direct methods, the structures were refined against F^2 with full-matrix least-squares using the program SHELXL-97.[25] All hydrogen atoms were placed in idealised positions and refined using a riding model.

Synthesis of 2

A solution was prepared by dissolving 65 mg (1.63 mmol) of NaOH in a mixture of 30 ml of EtOH and 4 ml of H_2O. 100 mg (0.20 mmol) of 2,5-bis(*N*-phenyl thioamide)-3,4-diphenylfuran were then added to this solution. The obtained suspension was dropwise added to a solution obtained by dissolving 257 mg (0.78 mmol) of $K_3[Fe(CN)_6]$ in 8 ml of H_2O. The mixture was vigorously stirred at reflux for 12 hours. The solvents were then removed under reduced pressure and the residual solids were dissolved in 30 ml CH_2Cl_2. The organic phase was then washed with water (3×25 ml) and dried over $MgSO_4$. After removal of the solvent under reduced pressure, the obtained solid was purified via column chromatography using a mixture of 5% toluene in CH_2Cl_2 as eluent, yielding **2** as a pale yellow solid. Single crystals suitable for X-ray diffraction were grown by slow evaporation of a concentrated ethyl acetate solution of **2** in a couple of days. Yield=33 mg (31%). Melting point 230.6-231.5 °C. Anal. calcd. for **2**·$(CH_2Cl_2)_{1/5}$: C 72.03, H 3.68, N 5.56; found: C 72.05, H 4.14, N 5.52. IR: ν=3063 m, 1546 m, 1505 m, 1463 m, 1429 s, 1312 s, 1262 s, 1235 s cm^{-1}. ^{1}H-NMR ($CDCl_3$): δ=8.08 (2H, d, *J*=8.0 Hz, benzothiazole-H), 7.89 (2H, d, *J*=8.0 Hz, benzothiazole-H), 7.48 (2H, dd, *J*=8.0 and 7.2 Hz, benzothiazole-H), 7.37-7.05 (12H, m br, benzothiazole-H and phenyl-H) ppm. ^{13}C-NMR ($CDCl_3$): δ=156.0, 153.5, 145.4, 135.0, 131.2, 130.3, 130.9, 128.9, 128.7, 126.6, 125.8, 124.0, 121.5 ppm.

Synthesis of 3

A solution was prepared by dissolving 32 mg (0.80 mmol) of NaOH in a mixture of 30 ml of EtOH and 4 ml of H_2O. 200 mg (0.56 mmol) of 2,5-bis(*N*-phenyl thioamide)thiophene were then added to this solution. The obtained suspension was dropwise added to a solution obtained by dissolving 760 mg (3.19 mmol) of $K_3[Fe(CN)_6]$ in 8 ml of H_2O. The mixture was vigorously stirred at reflux for 12 hours. The solvents were then removed under reduced pressure and the residual solids were dissolved in 20 ml of ethyl acetate. The organic phase was then washed with water (3x25 ml) and dried over $MgSO_4$. After removal of the solvent under reduced pressure, the obtained solid was purified via column chromatography using a mixture of 5% toluene in CH_2Cl_2 as eluent, yielding **3** as a pale yellow solid. Single crystals suitable for X-ray diffraction were grown by vapour diffusion of hexanes into a chloroform solution of **3**. Yield=25 mg (13%). Melting point 208.4-209.1 °C. Anal. calcd. for **3**·$(CH_2Cl_2)_{1/6}$: C 59.84, H 2.86, N 7.68; found: C 60.27, H 2.75, N 7.82. IR: ν=3065 m, 1546 m, 1505 m, 1429 s, 1237 s cm^{-1}. ^{1}H-NMR ($CDCl_3$): δ=8.06 (2H, d, *J*=8.0 Hz, benzothiazole-H), 7.88 (2H, d, *J*=8.0 Hz, benzothiazole-H), 7.68 (2H, br s, thiophene-$H_{3,4}$), 7.51 (2H, dd, *J*=8.0 and 7.2 Hz, benzothiazole-H), 7.40 (2H, dd, *J*=8.0 and 7.2 Hz, benzothiazole-H) ppm. ^{13}C-NMR ($CDCl_3$): δ=160.4, 153.9, 140.4, 135.1, 128.9, 126.8, 125.8, 123.5, 121.7 ppm.

Photophysical measurements

Absorption spectra were measured on a Varian Cary 5000 double-beam UV-Vis-NIR spectrometer and baseline corrected. Steady-state emission spectra were recorded on an Edinburgh FLSP920 spectrofluorimeter equipped with a 450 W Xenon arc lamp, double excitation and single emission monochromators, and a peltier cooled (253.15K) Hamamatsu R928P photomultiplier tube (185-850 nm). The excitation spectra were recorded by monitoring the maximum of the corresponding emission peaks. Emission and excitation spectra were corrected for source intensity (lamp and grating) and emission spectral response (detector and grating) by calibration curve supplied with the instrument. According to the approach described by Demas and Crosby,[26] luminescence quantum yields (Φ_{em}) were measured in optically dilute solutions (O.D. < 0.1 at excitation wavelength) obtained from spectra on a wavelength scale [nm] and compared to the reference emitter by the following equation:

$$\Phi_x = \Phi_r \left[\frac{A_r(\lambda_r)}{A_x(\lambda_x)}\right]\left[\frac{I_r(\lambda_r)}{I_x(\lambda_x)}\right]\left[\frac{n_x^2}{n_r^2}\right]\left[\frac{D_x}{D_r}\right]$$

where A is the absorbance at the excitation wavelength (λ), I is the intensity of the excitation light at the excitation wavelength (λ), n is the refractive index of the solvent, D is the integrated intensity of the luminescence and Φ is the quantum yield. The subscripts r and x refer to the reference and the sample, respectively. All quantum yields were performed at identical excitation wavelength for the sample and the reference, cancelling the $I(\lambda_r)/I(\lambda_x)$ term in the equation. All the compounds were measured against Rhodamine 101 in ethanol as reference.[27] Emission lifetimes were determined on the same Edinburgh instrument with the single photon counting technique (TCSPC) using pulsed picosecond LEDs (EPLED 295 or EPLED 360, FHWM <800 ps, repetition rates between 10 kHz and 1 MHz) as the excitation source; in each case, the above-mentioned R928P was used as detector. The goodness of fit was assessed by minimizing the reduced chi squared function (χ^2) and visual inspection of the weighted residuals. All solvents were of spectrometric grade and all solutions were filtered through a 0.2 mm syringe filter before measurement. Experimental uncertainties are estimated to be ±8% for lifetime determinations, ±20% for emission quantum yields, ±2 nm and ±5 nm for absorption and emission peaks, respectively.

The sample in polystyrene for the investigation of the solid-state photophysical properties of compound **1** was prepared by drop

casting a chloroform solution of **1** with a weight ratio of 0.1% of **1**-to-polystyrene (PS). The thickness of the film was about 500 μm and its maximum in absorption was 0.2–0.3. Absorption and emission spectra were recorded with the use of a Perkin Elmer Lambda 950 UV/Vis spectrophotometer and an Edinburgh FLS920 spectrofluorimeter, respectively. The photoluminescence was measured by a custom-made integrating sphere system attached to the same spectrofluorimeter, using the method of Friend.[28] Excited state lifetimes were obtained with an IBH500F time-correlated single-photon counting device.

OLED fabrication

Glass plates pre-coated with 150 nm-thick ITO (indium/tin oxide) with a sheet resistance of 20 Ω per square were used as substrates to grow a sequence of thin layers. All layers were deposited in succession by thermal evaporation under vacuum (~ 10^{-6} hPa), followed by the cathode layer consisting of 0.5 nm thick layer of LiF and 100 nm of Al. The current-voltage characteristics were measured with a Keithley Source-Measure unit, model 236, under continuous operation mode, while the light output power was measured with an EG&G power meter and the electroluminescence spectra were acquired with a Stellarnet spectroradiometer. All measurements were carried out at room temperature under argon atmosphere and were reproduced for many runs, excluding any irreversible chemical and morphological changes in the devices. The performance of the emissive layer (EML) has been optimised by locating it between exciton blocking layers of 4,4',4"-tri(9-carbazoyl)triphenylamine (TCTA) and 1,3,5-tri(1-phenyl-1H-benzo[d]imidazol-2-yl)benzene (TPBi), the latter acting also as an electron-transporting and hole-blocking layer.

Computational calculations

The molecular structures and the absorption spectra were calculated from first principles with the program GAUSSIAN 09[29] using the B3LYP hybrid functional and the 6-311++g** basis set. The absorption spectra were calculated within the time dependent density functional theory (TDDFT) formalism and the presence of the solvent (dichloromethane) was mimicked with the PCM implicit solvation model.[30] The 25 lowest excitation energies for each species were determined and the spectrum was produced by Gaussian functions with height proportional to the calculated intensities and a FWHM of 18 nm.

Results and discussion

Synthesis and characterisation

The synthesis of compound **1** was reported elsewhere.[22] In an analogous manner, compounds **2** and **3** were synthesised via oxidation of the corresponding 2,5-*N*-phenylthioamide-substituted furan and thiophene with $K_3[Fe(CN)_6]$ in an alkaline EtOH/H_2O mixture, as exemplified in Figure 2, followed by purification via column chromatography. The extent of reaction could be easily monitored with the use of thin layer chromatography, where the appearance of a blue-emitting spot under UV light reveals the formation of the benzothiazole moieties. The formation of the expected products **2** and **3** was also confirmed with the use of spectroscopic techniques. The disappearance in the ^{1}H-NMR of the secondary amide H peaks at 9.23 ppm (in $CDCl_3$) and 10.33 ppm (in d_6-DMSO) for **2** and **3** respectively, as well as the disappearance of one of the *ortho*-H signals in the aromatic region, indicated the successful cyclisation and formation of the benzothiazole heterocycles. Also, in the IR spectra the formation of the product is confirmed by the disappearance of the sharp NH peak around 3200 cm^{-1} for both initial substrates. Elemental analyses were also satisfactory for the purity of the compounds.

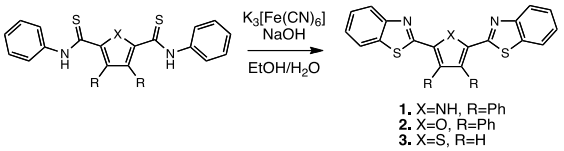

Figure 2. General methodology for the preparation of the dibenzothiazole compounds **1**, **2**, and **3**.

X-ray crystal structures of 2 and 3

The structural details of compound **1** were reported elsewhere.[22] A summary of the crystal data and structure refinement for the other two compounds is reported in Table 1. Compound **2** crystallises in the monoclinic *C*2/*c* space group and its structure is shown in Figure 3. One of the phenyl rings and one of the benzothiazole groups shows rotational disorder; these were modelled as split orientations using thermal parameter and geometrical restraints/constraints. The two benzothiazole units are oriented with the two N atoms on the same side of the molecule with respect to the furan O atom. Both benzothiazole units lie slightly distorted with respect the furan plane, with twisting angles ranging from 14° to 24°. Both phenyl rings are distorted with angles of approximately 80° with respect to the furan plane, in a similar fashion to the previously reported structure of **1**. There is very limited evidence of π-stacking throughout the lattice, whose formation seems to be somewhat hindered by the presence of the bulky phenyl rings in the 3 and 4 positions of the furan heterocycle.

Table 1. Crystal data and structure refinement details

	2	**3**
Empirical formula	$C_{30}H_{18}N_2OS_2$	$C_{18}H_{10}N_2S_3$
Formula weight	486.58	350.46
Temperature	120(2) K	120(2) K
Wavelength	0.71073 Å	0.71073 Å
Crystal system	Monoclinic	Monoclinic
Space group	*C*2/*c*	$P2_1/n$
Unit cell dimensions	*a*=26.3406(14) Å *b*=9.3058(5) Å *c*=19.5502(9) Å *β*=105.696(3)°	*a*=6.98500(10) Å *b*=20.4992(5) Å *c*=10.7665(3) Å *β* = 99.844(2)°
Volume	4613.5(4) $Å^3$	1518.92(6) $Å^3$
Z	8	4
Density (calculated)	1.401 Mg / m^3	1.533 Mg / m^3
Absorption coefficient	0.259 mm^{-1}	0.487 mm^{-1}
F(000)	2016	720
Crystal	Plate; Pale Orange	Block; Colourless
Crystal size	0.24 × 0.20 × 0.04 mm^3	0.13 × 0.04 × 0.03 mm^3
θ range for data collection	3.02 – 25.03°	3.12 – 25.02°
Index ranges	$-31 \le h \le 31$, $-11 \le k \le 9$, $-23 \le l \le 23$	$-8 \le h \le 8$, $-24 \le k \le 24$, $-12 \le l \le 12$
Reflections collected	28906	15141
Independent reflections	4070 [R_{int}=0.1214]	2685 [R_{int}=0.0773]
Completeness to *θ*= 25.03°	99.8 %	99.9 %
Absorption correction	Semi–empirical from equivalents	Semi–empirical from equivalents
Max. and min. transmission	0.9897 and 0.9405	0.9855 and 0.9394
Refinement method	Full-matrix least-squares on F^2	Full-matrix least-squares on F^2
Data / restraints / parameters	4070 / 26 / 213	2685 / 0 / 208
Goodness-of-fit F^2	1.074	1.125
Final *R* indices [$F^2 > 2\sigma(F^2)$]	*R1*=0.1334, *wR2*=0.2508	*R1*=0.0601, *wR2*=0.1108
R indices (all data)	*R1*=0.1960, *wR2*=0.2863	*R1*=0.0836, *wR2*=0.1224
Largest diff. peak and hole	1.065 and –0.606 e $Å^{-3}$	0.469 and –0.433 e $Å^{-3}$

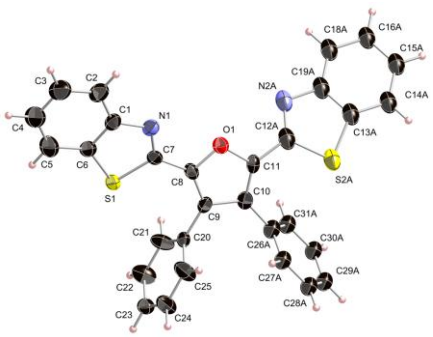

Figure 3. X-ray crystal structure of **2** with ellipsoids represented at 35% probability level and disordered atoms omitted for clarity.

Compound **3**, shown in Figure 4, crystallises into the monoclinic $P2_1/n$ space group. As in the case of **2**, the two benzothiazole units are arranged in order to localise the N atoms lying in a *cis* configuration with respect to the S atom of the thiophene ring. One of the

benzothiazole substituent lies essentially coplanar with the central thiophene group, whereas the second benzothiazole substituent is slightly twisted from planarity by a torsion angle of ca. 12°. There is limited π-stacking throughout the lattice involving adjacent benzothiazole units arranged to form infinite monodimensional layers of parallel molecules, with an interplanar distance of ca. 3.4 Å. Compared to the cases of **1** and **2**, the π-stacking of **3** is facilitated by the absence of the bulky phenyl substituents in the positions 3 and 4 of the thiophene ring. Within the layer, each unit is displaced so that only the benzothiazole units take part in the π-stacking arrangement. Neighbouring layers are arranged so that individual molecules almost lie perpendicular with respect to each other, as shown in Figure 5.

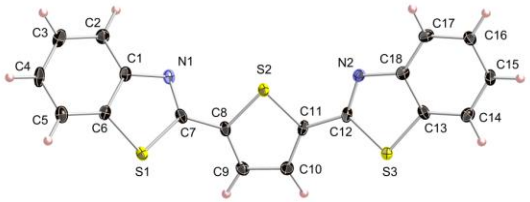

Figure 4. X-ray crystal structure of **3** with ellipsoids represented at 35% probability level.

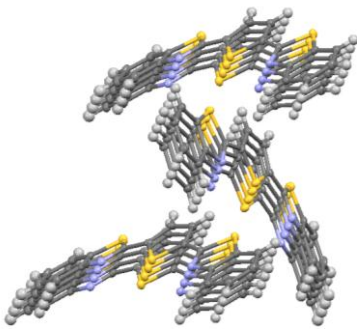

Figure 5. Layering structure in the lattice of **3**.

Photophysical Investigation

A summary of the photophysical data is reported in Table 2. The species **1**, **2**, and **3** display similar absorption and emission spectra, as shown in Figure 6, in diluted dichloromethane solutions (ca. 10^{-5} M). In particular, all the absorption plots consist of an intense band centered between 300 and 400 nm, together with a weaker and blue-shifted transition occurring between 254 and 291 nm. The lower energy band is ascribed to π-π* transitions, localised on the benzothiazole and heterocycle units. These can possibly be mixed by n-π* transitions of lower intensity, although they cannot be clearly distinguished from the spectra in solutions.

Table 2. Summary of the photophysical data from diluted (ca. 10^{-5} M) dichloromethane solutions.

	Absorption	**Emission, 298 K**		
	λ_{max}[nm] ($10^4\varepsilon$ [$M^{-1}cm^{-1}$])	**λ [nm]**	**τ [ns]**	**Φ**
1	291 (1.7) 384 (3.1) 405 (2.9)	444	1.76	0.42
1[a]		443	2	0.37
2	261 (2.3) 366 (6.8) 383 (7.7)	448	2.75	0.47
3	254 (0.6) 374 (4.5) 394 (2.9)	450	1.80	0.21

[a] from a polystyrene matrix doped with **1** (0.1%).

In all cases, the π-π* absorption band displays a distinct vibronic progression, with a separation between adjacent resolved peaks of the order of 1,350-1,200 cm^{-1}. Previously reported electronic absorption profiles for similar substrates, possessing benzothiazole units connected to five-membered heterocylic substituents, but lacking the C_2 symmetry, showed absorption bands almost devoid of vibrational structures.[21] In those cases, the structureless shape of the bands was attributed to a relatively high degree of rotational freedom for the bond connecting the benzothiazole units to the heterocycles, this effect being observed even in low-polarity solvents such

as methylcyclohexane. The appearance of vibrational features in **1**, **2**, and **3** might be due to increased rigidity in the compounds reported here. The blue-shifted higher-energy band is ascribed to a combination of π-π* transitions involving the two phenyl rings attached to the central heterocycles. The quasi-perpendicular arrangement of the phenyl substituents with respect to the central heterocycles significantly reduces the extent of interannular conjugation and the degree of delocalization, thus the electronic behaviour of the two systems are likely to be almost independent of each other. This hypothesis is supported by the fact that in the absorption profile of compound **3**, which does not possess the phenyl substituents in the 3 and 4 positions of the thiophene ring, this higher-energy band is almost absent with respect to compounds **1** and **2**. The absorption maxima of the benzothiazole units in the three compounds do not seem to vary significantly upon changing the heterocyclic core. The most notable shift with $\Delta\lambda_{max}$=10 nm occurs on comparing **1** and **2**, which have almost identical maxima at λ_{max}(**1**)=384 nm and λ_{max}(**2**)=383 nm, with respect to **3**, for which λ_{max}(**3**) is blue-shifted to 374 nm. While more pronounced shifts were previously reported on changing the substituent on the benzothiazole unit from pyrrole to thiophene,[21] in this case the heterocycle is linking two symmetrically equivalent benzothiazole units and its electronic effect on each benzothiazole is therefore likely to be reduced.

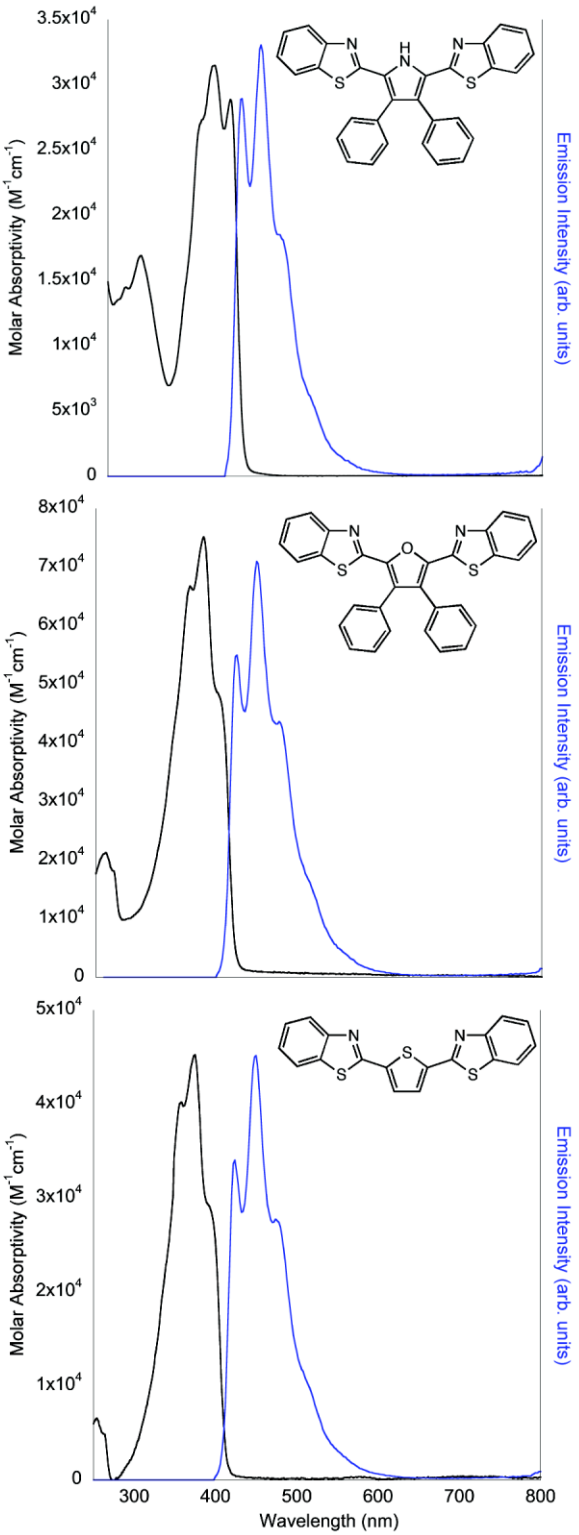

Figure 6. Absorption (black) and emission (blue) plots of a diluted (10^{-5} M) dichloromethane solution of **1**, **2**, and **3**.

Upon excitation at 360 nm, compounds **1**, **2** and **3** display bright luminescence with blue-coloured emission maxima centred in the range 444-459 nm (Figure 6). In particular, all the emission spectra show a resolved vibrational structure mirroring with the absorption profiles. All the compounds exhibit a variable degree of overlap between the absorption and emission profiles, with the lowest Stokes shift visible for compound **1**. The photoluminescence of **1** was also trialled by using polystyrene (PS) as a host matrix with concentration of the dopant at 0.1%. The absorption and emission profiles in the solid matrix are very similar to the ones measured from dichloromethane solutions (see ESI, Figure S2).

The excited state lifetimes of the three species are characteristic of spin-allowed radiative decays (fluorescence) with values between 1 and 3 ns. The values of the quantum yield for species **1** and **2**, possessing the two phenyl rings attached to the central heterocycle, are 42% and 47% respectively. On the other hand, compound **3** exhibits a reduced quantum yield of 21%. The lower quantum yield of **3** is tentatively ascribed to the presence of the extra S atom in the thiophene ring, which could favour some degree of intersystem crossing between the lowest singlet and triplet excited states in competition with radiative decay. This effect has been previously reported for analogous porphyrinic systems.[31]

DFT calculations

To obtain more insight into the photophysical properties of the compounds, DFT calculations were performed. In general, the simulated absorption profiles for **1**, **2**, and **3** (shown in ESI, Figure S1) are in qualitative agreement with the experimental data. The relaxed geometries for all the three compounds evidence a planar arrangement, thus favouring extended delocalization of the π-electrons and enhancing the rigidity of the species in solution. This result is in agreement with the resolved vibrational structures observed in the experimental absorption spectra. The calculated profiles highlight an intense lower-energy band followed by a less intense higher-energy band, the latter more pronounced for **1**, and **2**. According to the data, the major contributor to the lower-energy band is a HOMO-LUMO transition, both of which lie localised between the central heterocycle and the five-membered units of both benzothiazole substituents (Figure 7). The contours of these orbitals are identical is all three cases. For **1** and **2**, the higher-energy transitions originate from orbitals localised on the phenyl rings to π* orbitals localised on the central heterocycle, suggesting transitions with partial charge transfer character.

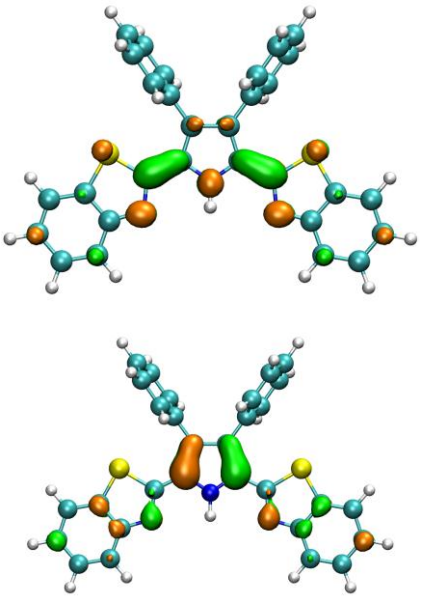

Figure 7. Molecular orbital contours highlighting the LUMO (top) and HOMO (bottom) for species **1**.

Electroluminescence and OLED fabrication using 1 as a blue-emissive dopant

Given that, compound **1** can be obtained in higher yields, the steady-state emission profiles are very similar for the three species, and the quantum yield of **3** is inferior with respect to **1** and **2**, we have decided to use **1** as a dopant for the fabrication of blue OLEDs. The electroluminescence of compound **1** was employed in two multilayer OLEDs as fluorescent emitter. In both cases, the device architecture and composition adopted was ITO/MoO_3 (2 nm)/TCTA (80 nm)/EML (30 nm)/TPBi (30 nm)/LiF (0.5 nm)/Al (100 nm). In the first device, the EML was obtained by blending **1** in TCTA at a concentration equal to 4% w/w. For comparison, a second device was prepared with the emitting layer being composed of 100% **1**, as a neat film. Figure 8 displays the performances of both devices, the brightness as a function of the driving voltage and the external electroluminescent quantum efficiency as function of the current density (j). Maximum luminance reaches 2500 cd/m^2 and 650 cd/m^2 at about 100 mA/cm^2 for EML=4% of **1** in TCTA and EML=100% of **1**, respectively. The external quantum efficiency for the device where EML=4% of **1** in TCTA is ~ 2.5% at low current density, which corresponds to the theoretical upper limit when the light extraction factor is assumed to be ¼ of the total emission. In the case of the device with a neat film as EML, the external quantum efficiency is of the order of 0.1%, suggesting that the emitting material undergoes self–quenching when forming aggregate species. The higher roll-off effect of the OLED with a low concentration of emitter, compared to the neat film as EML, as shown in Figure 8, suggests a more efficient effect of the excitonic dissociation by the electric field on the molecular excited state than on aggregate species.[32]

The electroluminescence spectra of both devices are reported in Figure 9. No contribution to the electroluminescence emission from the TCTA binder or from the TPBi electron-transport layer is observed. The absence of the TCTA and TPBi emission indicates that the

excitons are confined to the EML, where they are localised on the fluorescent molecule prior to radiative emission. The electroluminescence of **1** blended in TCTA is of deep-blue colour and results in a slight red–shift (λ_{max}=458 nm) in relation with both solution and dispersion into a polystyrene matrix (λ_{max}=444 nm and 443 nm, respectively). This red-shift effect could be attributed to a partial charge transfer character of excited state, which would be influenced by the polarity of the surrounding medium.

The device with the neat film of **1** as emitting layer displays emission characteristics consistent with the formation of aggregate species, arising from interaction of neighbouring molecules. The electroluminescent emission of this device is broad, almost structureless and with a maximum at lower energies (λ_{max}~600 nm) with respect to the other OLED. It is possible to distinguish a small contribution as a shoulder of the single molecule emission in the high-energy region of the band between 400 and 500 nm. The combination of these two emission profiles, from the single molecules of **1** and aggregates, allows coverage of most of the visible spectrum, thus the neat-film device yields white emission, with CIE coordinates of x=0.381 and y=0.400 (see Figure 9) as well as CRI=86 (Colour Rendering Index).[33] Various strategies have been reported in the literature in order to obtain white light in OLEDs using a single molecule as dopant to simplify the fabrication process (instead of a balanced mixture of the blue, red, and green primary colours).[34] As evidenced by the electroluminescent data, compound **1** allows white emission from the formation of aggregates, however this also results in a lower efficiency due to self-quenching effects.

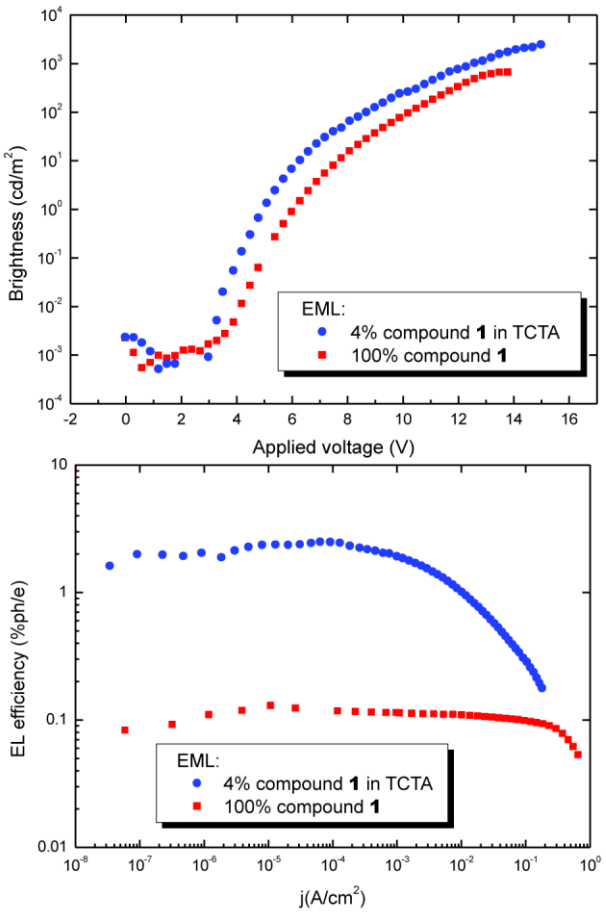

Figure 8. Brightness *vs.* voltage plot (top); EL Quantum Efficiency vs. electric current density.

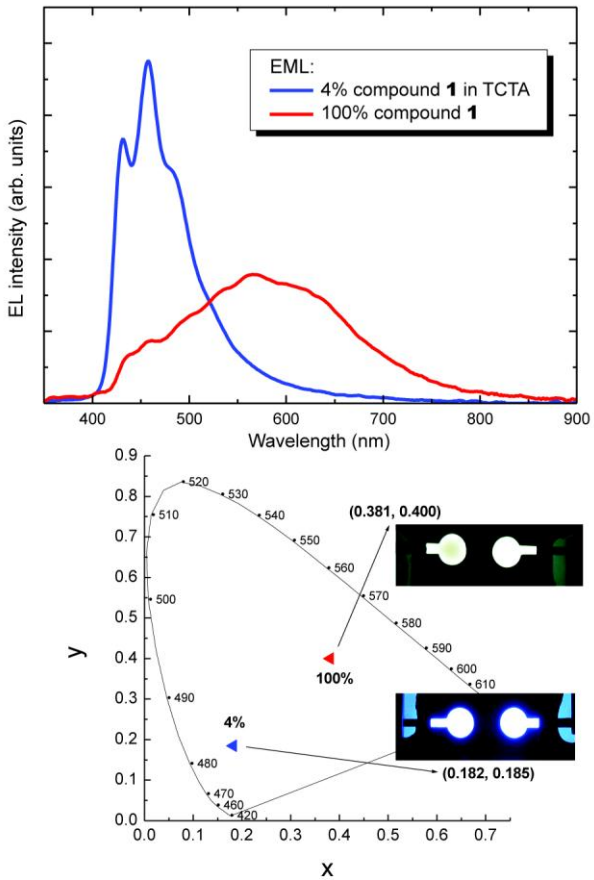

Figure 9. EL spectra of the OLED devices (top); CIE coordinates and photos of the OLEDs (bottom) where the blue triangle refers to the EML made of 4% of **1** in TCTA and the red triangle refers to the EMLs made of a neat film of **1**.

Conclusions

In conclusion, the photophysical properties of C_2-symmetrical dibenzothiazolyl substituted pyrrole, furan, and thiophene have been investigated, revealing blue emission originating from electronic π-π* excited states. The quantum yield of the emission was found to be higher in the case of pyrrole and furan with respect to thiophene, which was tentatively attributed to the presence of the S atom in the heterocycle. Due to its more efficient synthesis and good quantum yield, the pyrrole **1** compound was used as dopant in the fabrication of OLED architectures. Using 4% of **1** blended with TCTA yielded devices with deep-blue emission. On the other hand, using **1** as a neat film in the emissive layer yielded devices characterised by white light emission as a consequence of aggregation, however this also caused a drop in quantum efficiency originating from self-quenching effects.

Acknowledgments

The work was supported by the Australian Research Council. MM wishes to thank the ARC for the APD Fellowship (DP0985481). PR thanks the ARC for the ARF fellowship (DP 0986999) and iVEC and the National Computational Infrastructure for the provision of computer time. The OLED work was supported by Consorzio MIST E-R (project FESR-Tecnopolo AMBIMAT). Dr. Massimo Cocchi (ISOF, Bologna, Italy) is kindly acknowledge for useful discussion and help with the fabrication of the OLED.

Notes and references

[a] *Department of Chemistry, Curtin University, Kent Street, Bentley 6102 WA, Australia; E-mail: m.massi@curtin.edu.au*
[b] *Chemistry, University of Southampton, Southampton, UK, SO17 1BJ.*
[c] *Department of Physical and Inorganic Chemistry, University of Bologna, viale del Risorgimento 4, 40126, Bologna, Italy; E-mail: stefano.stagni@unibo.it*
[d] *Consorzio MIST E-R, via P. Gobetti 101, 40129 Bologna, Italy.*
† Electronic Supplementary Information (ESI) available: selected bond lengths and angles for **2** and **3**; calculated absorption profiles, list of transitions, and frontier orbital contours for **1**, **2**, and **3**. See DOI: 10.1039/b000000x/

1. D. Yao, S. Zhao, J. Guo, Z. Zhang, H. Zhang, Y. Liu and Y. Wang, *J. Mater. Chem.*, 2011, **21**, 3568-3570.
2. J.-G. Kang, H.-J. Kim, Y.-K. Jeong, M.-K. Nah, C. Park, Y. J. Bae, S. W. Lee and I. T. Kim, *J. Phys. Chem. B*, 2010, **114**, 3791-3798.
3. J. Pina, J. S. Seixas de Melo, H. D. Burrows, R. M. F. Batista, S. P. G. Costa and M. M. M. Raposo, *J. Phys. Chem. A*, 2007, **111**, 8574-8578.
4. S. M. Chang, Y. J. Tzeng, S. Y. Wu, K. Y. Li and K. L. Hsueh, *Thin Solid Films*, 2005, **477**, 38-41.
5. R. M. F. Batista, S. P. G. Costa and M. M. M. Raposo, *Tetrahedron Lett.*, 2004, **45**, 2825-2828.
6. P. Yang, J. Z. Zhao, W. H. Wu, X. R. Yu and Y. F. Liu, *J. Org. Chem.*, 2012, **77**, 6166-6178.
7. R. J. Wang, D. Liu, H. C. Ren, T. Zhang, X. Z. Wang and J. Y. Li, *J. Mater. Chem.*, 2011, **21**, 15494-15500.
8. R. Czerwieniec, A. Kapturkiewicz, J. Lipkowski and J. Nowacki, *Inorg. Chim. Acta*, 2005, **358**, 2701-2710.
9. S. P. Y. Li, T. S. M. Tang, K. S. M. Yiu and K. K. W. Lo, *Chem. Eur. J.*, 2012, **18**, 13342-13354.
10. J. Kuwabara, T. Namekawa, M. Haga and T. Kanbara, *Dalton Trans.*, 2012, **41**, 44-46.
11. M. A. Katkova, A. P. Pushkarev, T. V. Balashova, A. N. Konev, G. K. Fukin, S. Y. Ketkov and M. N. Bochkarev, *J. Mater. Chem.*, 2011, **21**, 16611-16620.
12. N. M. Shavaleev, R. Scopelliti, F. Gumy and J. C. G. Bunzli, *Inorg. Chem.*, 2009, **48**, 6178-6191.
13. M. K. Nah, S. G. Rho, H. K. Kim and J. G. Kang, *J. Phys. Chem. A*, 2007, **111**, 11437-11443.
14. R. M. F. Batista, S. P. G. Costa, M. Belsley and M. M. M. Raposo, *Tetrahedron*, 2007, **63**, 9842-9849.
15. S. P. G. Costa, R. M. F. Batista, P. Cardoso, M. Belsley and M. M. M. Raposo, *Eur. J. Org. Chem.*, 2006, 3938-3946.
16. Y. V. Fedorov, O. Fedorova, N. Schepel, M. Alfimov, A. M. Turek and J. Saltiel, *J. Phys. Chem. A*, 2005, **109**, 8653-8660.
17. A. Mabrouk and A. A. K. Alimi, *J. Phys. Chem. Solids*, 2010, **71**, 1225-1235.
18. H. Y. Fu, X. D. Gao, G. Y. Zhong, Z. Y. Zhong, F. Xiao and B. X. Shao, *J. Luminesc.*, 2009, **129**, 1207-1214.
19. X. H. Zhang, O. Y. Wong, Z. Q. Gao, C. S. Lee, H. L. Kwong, S. T. Lee and S. K. Wu, *Mat. Sci. Eng. B*, 2001, **85**, 182-185.
20. R. M. F. Batista, S. P. G. Costa, E. L. Malheiro, M. Belsley and M. M. M. Raposo, *Tetrahedron*, 2007, **63**, 4258-4265.
21. J. Pina, J. Sérgio Seixas de Melo, R. M. F. Batista, S. P. G. Costa and M. M. M. Raposo, *Phys. Chem. Chem. Phys.*, 2010, **12**, 9719.
22. L. E. Karagiannidis, P. A. Gale, M. E. Light, M. Massi and M. I. Ogden, *Dalton Trans.*, 2011, **40**, 12097.
23. G. W. Bates, P. A. Gale, M. E. Light, M. I. Ogden and C. N. Warriner, *Dalton Trans.*, 2008, 4106-4112.
24. P. A. Gale, S. Camiolo, G. J. Tizzard, C. P. Chapman, M. E. Light, S. J. Coles and M. B. Hursthouse, *J. Org. Chem.*, 2001, **66**, 7849-7853.
25. G. M. Sheldrick, *Acta Cryst.*, 2008, **A64**, 112-122.
26. G. C. Crosby and J. N. Demas, *J. Phys. Chem.*, 1971, **75**, 991-1024.
27. T. Karstens and K. Kobs, *J. Phys. Chem.*, 1980, **84**, 1871-1872.
28. J. C. de Mello, H. F. Wittmann and R. H. Friend, *Adv. Mater.*, 1997, **9**, 230-232.
29. M. J. Frisch, G. W. Trucks, H. B. Schlegel, G. E. Scuseria, M. A. Robb, J. R. Cheeseman, G. Scalmani, V. Barone, B. Mennucci, G. A. Patersson, H. Nakatsuji, M. Caricato, X. Li, H. P. Hratchian, A. F. Izmaylov, J. Bloino, G. Zheng, J. L. Sonnengerg, M. Hada, M. Ehara, K. Toyota, R. Fukuda, J. Hasegawa, M. Ishida, T. Nakajima, Y. Honda, O. Kitao, H. Nakai, T. Vreven, J. Montgomery, J. A., J. E. Peralta, F. Ogliaro, M. Bearpark, J. J. Heyd, E. Brothers, K. N. Kudin, V. N. Staroverov, R. Kobayashi, J. Normand, K. Raghavachari, A. Rendell, J. C. Burant, S. S. Iyengar, J. Tomasi, M. Cossi, N. Rega, J. M. Millam, M. Klene, J. E. Knox, J. B. Cross, V. Bakken, C. Adamo, J. Jaramillo, R. Gomperts, R. E. Stratmann, O. Yazyev, A. J. Austin, R. Cammi, C. Pomelli, J. W. Ochterski, R. L. Martin, K. Morokuma, V. G. Zakrzewski, G. A. Voth, P. Salvador, J. J. Dannenberg, S. Dapprich, A. D. Daniels, O. Farkas, J. B. Foresman, J. V. Ortiz, J. Cioslowski and D. J. Fox, *Gaussian 09, Revision B.01*, Wallingford CT, 2009.
30. J. Tomasi, B. Mennucci and R. Cammi, *Chem. Rev.*, 2005, **105**, 2999-3093.
31. J.-H. Ha, S. Ko, C.-H. Lee, W.-Y. Lee and Y.-R. Kim, *Chem. Phys. Lett.*, 2001, **349**, 271-278.
32. J. Kalinowski, M. Cocchi, V. Fattori, L. Murphy and J. A. G. Williams, *Org. Electron.*, 2010, **11**, 724-730.
33. J. H. Jou, S. M. Shen, C. R. Lin, Y. S. Wang, Y. C. Chou, S. Z. Chen and Y. C. Jou, *Org. Electron.*, 2011, **12**, 865-868.
34. M. Cocchi, J. Kalinowski, L. Murphy, J. A. G. Williams and V. Fattori, *Org. Electron.*, 2010, **11**, 388-396.